frontiers | Frontiers in Materials

ORIGINAL RESEARCH
published: 29 June 2022
doi: 10.3389/fmats.2022.931848

Effects of Grain Boundary Engineering on the Microstructure and Corrosion Fatigue Properties of 316L Austenitic Stainless Steel

Mingxian Zhang[1,2], *Chenxin Zhang*[3], *Huanchun Wu*[4] *and Bin Yang*[5]*

[1]School of Physics and Materials Science, Nanchang University, Nanchang, China, [2]International Institute for Materials Innovation, Nanchang University, Nanchang, China, [3]China Nerin Engineering Company Limited, Nanchang, China, [4]Plant Life Management Center, Suzhou Nuclear Power Research Institute, Suzhou, China, [5]Collaborative Innovation Center of Steel Technology, University of Science and Technology Beijing, Beijing, China

Grain boundary engineering (GBE) treatment was performed through thermomechanical processing (TMP) to optimize the grain boundary character distribution (GBCD) of 316L austenitic stainless steel. The effects of TMP on the GBCD and corrosion fatigue properties in high-temperature and high-pressure water were investigated. The results indicated that a high fraction (about 74%) of special boundaries as well as the interrupted network of random high-angle grain boundaries were obtained through 5% strain followed by annealing at 1,273 K for 90 min. The Σ9 and Σ27 boundaries were generated by the reaction of special boundaries. The highest corrosion fatigue life for 3,187 cycles was obtained when the TMP parameters of the 316L ASS were of 5% strain, annealing temperature of 1,273 K, and annealing time of 45 min. The low-energy special boundaries had strong intergranular corrosion resistance, but the strength of these boundaries was not enough to resist the propagation of transgranular fatigue cracks.

Keywords: grain boundary engineering, thermomechanical processing, grain boundary character distribution, special boundaries, corrosion fatigue

OPEN ACCESS

Edited by:
Jie Qiu,
Xi'an Jiaotong University, China

Reviewed by:
Xin Dai,
North China University of Science and Technology, China
Fang Wang,
Nanchang Hangkong University, China

***Correspondence:**
Bin Yang
byang@ustb.edu.cn

Specialty section:
This article was submitted to Environmental Degradation of Materials, a section of the journal Frontiers in Materials

Received: *29 April 2022*
Accepted: *09 May 2022*
Published: *29 June 2022*

Citation:
Zhang M, Zhang C, Wu H and Yang B (2022) Effects of Grain Boundary Engineering on the Microstructure and Corrosion Fatigue Properties of 316L Austenitic Stainless Steel. Front. Mater. 9:931848. doi: 10.3389/fmats.2022.931848

INTRODUCTION

316L austenitic stainless steel (ASS) has been widely used in petrochemical, chemical, power, and nuclear industries (Wang, 2019). However, the links between the grains of ASS are usually weak. GB-related cracks always result in the failure of 316L ASS in the corrosive environments. Therefore, the type, the frequency, and the character of the grain boundaries should be optimized to improve the properties of the steel.

Grain boundary engineering (GBE) as an approach of grain boundary design and control was first proposed by Tadao Watanabe (1984). According to the principle of GBE, the enhancement of grain boundary failure resistance can be attributed to the increase of special boundaries (SBs) and the redistribution of the grain boundary network. The structure of grain boundaries has commonly been described by the coincidence site lattice (CSL) model based on the misorientation between the neighboring grains. Grain boundaries can be categorized by "sigma value (Σ)" into two families. They are the SBs whose sigma value are ≤ 29 according to the Brandon criterion and others which are random high-angle grain boundaries (RHAGBs). Compared to the RHAGBs, the SBs are usually difficult to be degraded due to their higher ordering degree, closer atomic packing, smaller free volume, and lower interface energies. It is generally considered that material with high frequency of SBs has a high resistance to the intergranular deterioration, especially coherent ∑3 boundaries.

Thermomechanical processing (TMP) comprising a combination of prior deformation and consequent annealing has been commonly considered as a successful GBE method (Engelberg, 2008). The TMP can significantly increase the fraction of the ordered-structure GBs and effectively optimize the grain boundary character distribution (GBCD) (Li, 2009; Sinha, 2015; Kang, 2021). As a result, the properties related to GBs can be greatly improved. In recent years, several research studies have proved that the application of GBE could significantly enhance the resistance to intergranular corrosion (Lehockey, 1997; Shimada, 2002), hot corrosion (Deepak, 2016), stress corrosion cracking (Gertsman, 2001; West, 2009), fatigue (Kobayashi, 2011), creep (Thaveeprungsriporn, 1997; Spigarelli, 2003), and embrittlement (Watanabe, 1999).

The influence of GBE on the corrosion fatigue properties has been seldom studied due to the combined effects of the intergranular corrosion and fatigue. Lehockey (Lehockey, 1998) showed that the increases in corrosion, creep, and fatigue resistance ranging between 40 and 90 pct could be achieved by increasing the relative proportion of crystallographically "special" low-Σ CSL boundaries in the microstructure of superalloys V-57 and 738. Kobayashi (Kobayashi, 2020) investigated the roles of GBs in fatigue-crack nucleation and propagation of 430 ferritic stainless steel, 316L, and 304 austenitic stainless steel. It was shown that the crack propagation rate of Σ3 boundaries was lower than that of RHAGBs when the cracks propagated along the boundaries. The fatigue strength and fatigue life of those steels could be increased by raising the fraction of CSL boundaries.

However, Gao (Gao, 2005; Gao, 2007) explored the influence of SBs character on the propagation of the small cracks of ME3 superalloy. He held the opinion that SBs were not more effective than RHAGBs in impeding the fatigue-crack propagation primarily. Because the crack advance was predominantly transgranular, Mohtadi-Bonaba (Mohtadi-Bonaba, 2018) investigated the microstructural aspects of intergranular and transgranular fatigue-crack propagation of X65 steel. It was observed that SBs acted as high-energy boundaries during crack propagation due to an accumulation of Σ3 boundaries around the fatigue microcracks. Gao (Gao et al., 2019) investigated the corrosion fatigue behavior of 316LN ASS in borated and lithiated high-temperature water. The results showed that the fatigue life of the material was mainly attributed to the grain size rather than the fraction of SBs due to their inapparent resistance to transgranular cracking. It could be concluded that the variation law and mechanisms of the GBE process on the microstructure and corrosion fatigue properties of 316L ASS should be studied clearly.

In this article, the effects of TMP parameters with the type of compression-annealing on the GBCD and the corresponding mechanism in 316L austenitic stainless steel were studied. Meanwhile, the effects of GBE on the corrosion fatigue properties of 316L ASS in high-temperature (563 K) and high-pressure (8 MPa) water were also investigated.

EXPERIMENT

AISI 316L austenitic stainless steel was chosen in the study. The chemical composition (wt%) of the steel was 17.4 Cr, 13.58 Ni, 2.14 Mo, 1.60 Mn, 0.53 Si, 0.024 C, 0.01 P, 0.01 N, and 0.013 S. The steel was solution-treated at 1,373 K for 1 h followed by water quenching to normalize the microstructure. The cylindrical specimens with a diameter of 20 mm and height of 30 mm were manufactured after the solution treatment. Then, the TMP composed of unidirectional compression and subsequent annealing followed by quenched in cold water (298 K) was carried out. The compression was 5%. The annealing treatment was conducted at 1,273 K for 10–90 min in the study. The sliced specimens were perpendicular to the compression axis. The surfaces of slices were grinded with 2,000-grit abrasive paper and then electropolished in an electrolyte consisting of 20% perchloric acid and 80% alcohol at 30 V for 30 s.

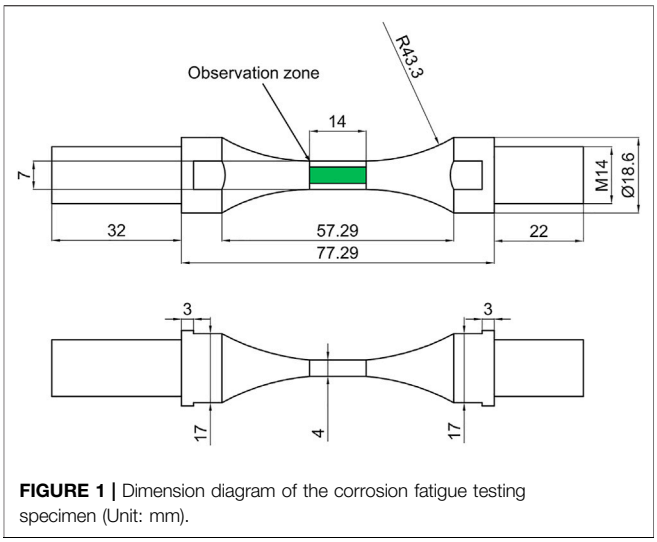

FIGURE 1 | Dimension diagram of the corrosion fatigue testing specimen (Unit: mm).

The orientation imaging microscopy (OIM) of the specimens was analyzed by electron back-scattered diffraction (EBSD) technique which was performed by a Zeiss Auriga field-emission scanning electron microscope (SEM) equipped with the HKL-Channel 5 EBSD system. The operating conditions of SEM were 20 kV accelerating voltage, 16.5 mm working distance, 70 beam incidence angle, and 2 μm step size. The EBSD data were analyzed using Channel 5 software from Oxford-HKL. The grain boundaries were categorized as the sub-boundaries, low-angle boundaries (Σ1 boundaries), and high-angle boundaries. When the misorientation range was from 2° to 5°, the boundaries were considered as the sub-boundaries. When the misorientation range was from 5° to 15°, the boundaries were considered as the low-angle boundaries (i.e., Σ1 boundaries). When the misorientation range was above 15°, the boundaries were considered as the high-angle boundaries. Brandon's criterion ($\Delta\theta = 15/\Sigma 1/2$) was adopted for the critical deviation in the characterization of grain boundaries. The grain boundaries whose Σ-value range was from 1 to 29 were regarded as low-Σ CSL boundaries (i.e., SBs). In the OIM figures, the RHAGBs were represented by the black lines. The Σ3 twin boundaries and the other SBs were represented by the red and the other colored lines, respectively. The fractions of grain boundaries were determined in terms of the length fraction by dividing the number of pixels of a particular boundary with that of the entire grain boundaries.

TABLE 1 | The conditions of the corrosion fatigue test.

Water temperature (K)	Water pressure (MPa)	Wave form	Strain amplitude	Strain rate (s)	Dissolved oxygen (ppm)	pH	Conductivity
563	8	Triangle	±0.5%	0.001^{-1}	10	6.6	0.15 μs/cm

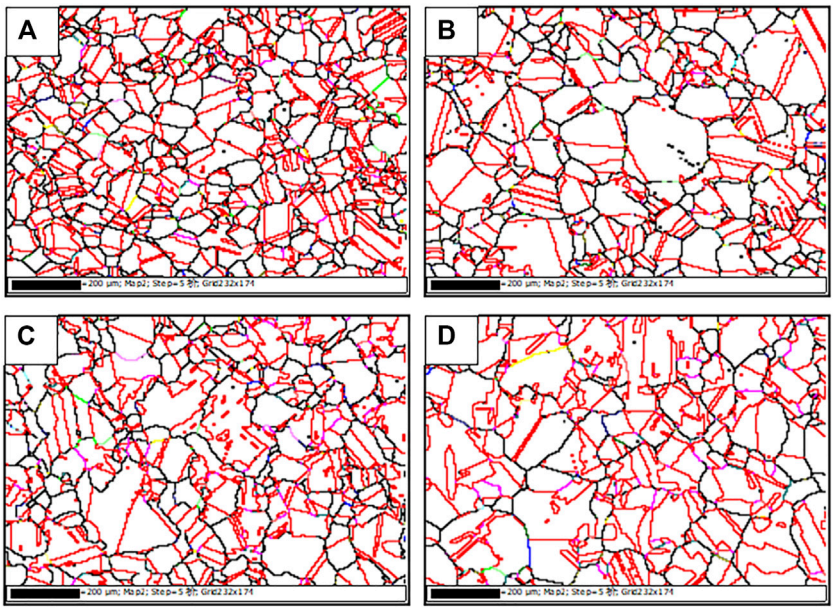

FIGURE 2 | GBCD of the **(A)** initial specimen and the GBE-treated specimens annealed for **(B)** 10 min, **(C)** 45 min, and **(D)** 90 min.

Before the corrosion fatigue tests, the sensitization treatment of the specimens was carried out at 973 K for 48 h. According to the standard of ASTME 606, the dimensions of the specimens are shown in **Figure 1**. The flat planes in the gauge position were machined in each specimen to observe the microstructure after the CF test. The corrosion fatigue (CF) tests were conducted in the CF instrument with a computer-controlled servo electric system. The test conditions were listed in **Table 1**. The strain control mode with fully reversed triangular waveform was chosen. The capacity dynamic load was 20 kN. The SS static auto clave was adopted. The strain was measured by using an extensometer. The solution was prepared using distilled water. The temperature was 563 K, and the pressure was 8 MPa. The fatigue life was defined in terms of the number of cycles when the peak tensile stress was dropped to 75% of the maximum peak stress.

RESULTS AND DISCUSSION

Effect of GBE on the GBCD of 316L ASS

The OIM was performed to investigate the GBCD of each specimen. The GBCD of the four specimens composed of the initial specimen and the GBE-treated specimens is shown in **Figure 2**. It can be observed from **Figure 2A** that the microstructure of the initial specimen was relatively homogeneous. The grains were surrounded by RHAGBs. The straight SBs mainly composed of straight coherent Σ3 boundaries were almost inside the grains. When the annealing time of the GBE-treated specimen was 10 min, it can be observed in **Figure 2B** that the morphology of the SBs was almost unchanged. Most SBs were still straight and existed in the grains. As the annealing time increased to 45 min, the short and curved boundaries appeared in **Figure 2C**. Some SBs became a part of the grain boundary network. A significant increase of the SBs number can be also observed. When the annealing time increased to 90 min, the number of SBs increased significantly, especially the short and curved one. Meanwhile, the grain size of the specimen reached the maximum. Compared to the aforementioned microstructure, more parts of grain boundaries were replaced by the SBs, as seen from **Figure 2D**.

To study the connectivity of RHAGBs' network of these specimens, only the RHAGBs (black lines) remained in **Figure 3**. **Figure 3A** shows that the average grain size of the initial specimen was about 97 μm. The RHAGBs' network of the initial specimen was significantly interconnected because most SBs did not take part in the grain boundary network. When the annealing time increased to 10 min, it can be seen in **Figure 3B** that the grain size of the specimen increased evidently compared to the initial specimen, whereas the RHAGBs were still interconnected. As the annealing time increased to 45 min, the connection of RHAGBs was interrupted sparingly, as shown in **Figure 3C**. When the annealing time increased to 90 min, the grain size of the specimen reached the maximum. Moreover, the connected network of RHAGBs was disrupted significantly, as shown in **Figure 3D**.

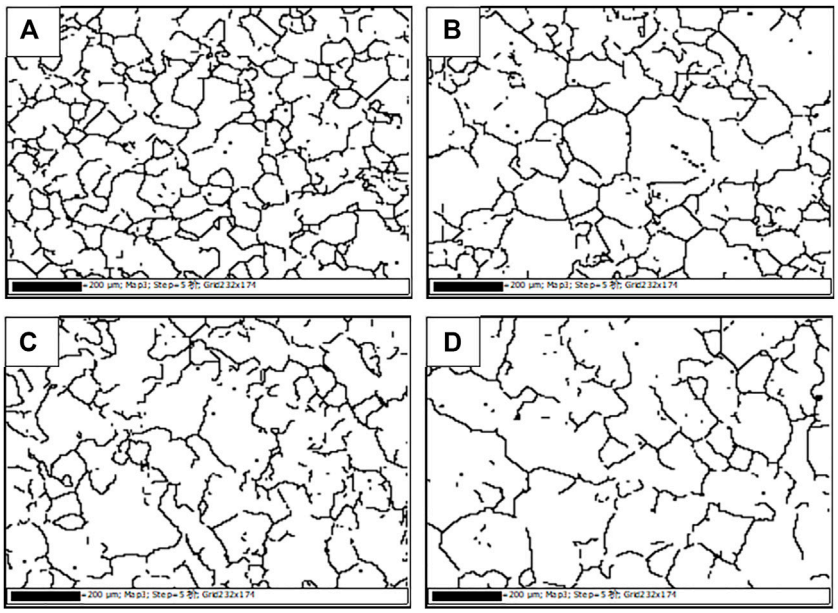

FIGURE 3 | The RHAGBs network of the **(A)** initial specimen and the GBE-treated specimens annealed for **(B)** 10 min, **(C)** 45 min, and **(D)** 90 min.

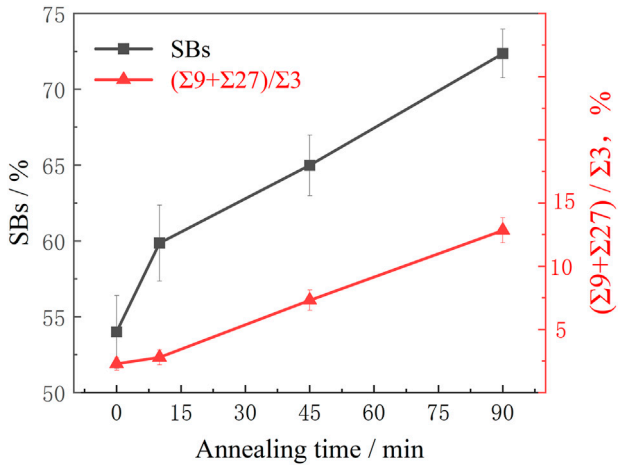

FIGURE 4 | The curves of the SBs' (Σ1–Σ29) percentages and the (Σ9 + Σ27)/Σ3 ratios.

The curves of the SBs' (Σ1–Σ29) percentages and the (Σ9 + Σ27)/Σ3 ratios under different annealing times were shown in **Figure 4**. It could be seen that the percentage of the SBs increased gradually with the increase of the annealing time. The SBs fraction of the initial specimen and the specimen annealing for 90 min were 55% and 74%, respectively. The ratio of (Σ9 + Σ27)/Σ3 was shown to follow the similar continuous growth trend, especially when the annealing time was from 10 to 90 min. When the annealing time was 90 min, the (Σ9 + Σ27)/Σ3 ratio reached its maximum.

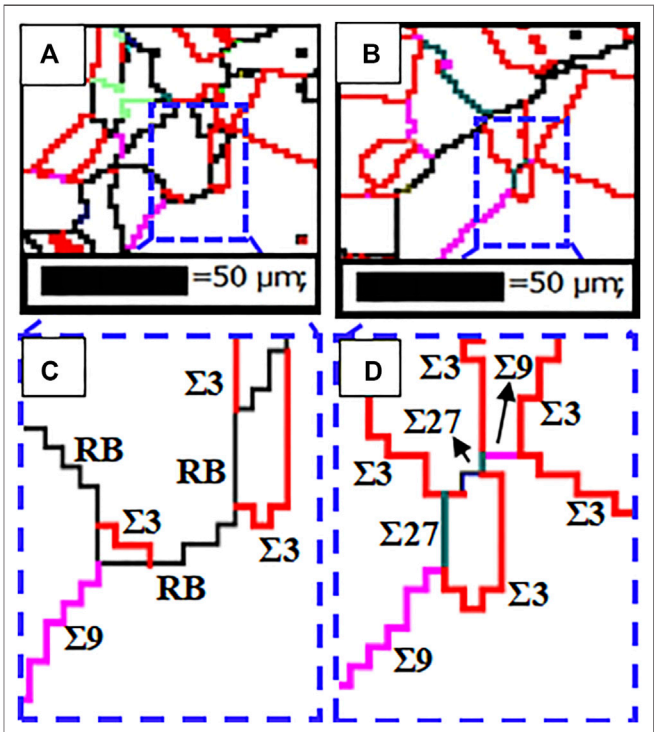

FIGURE 5 | The OIM map of the same region in the GBE-treated specimen annealed for **(A)** 45 min and **(B)** 90 min; **(C)** local enlarged drawing of **(A)**; **(D)** local enlarged drawing of **(B)**.

To investigate the generation mechanism of the SBs during the annealing, the GBCD evolution of the fixed region in the GBE-treated specimens was observed, as shown in **Figure 5**. It

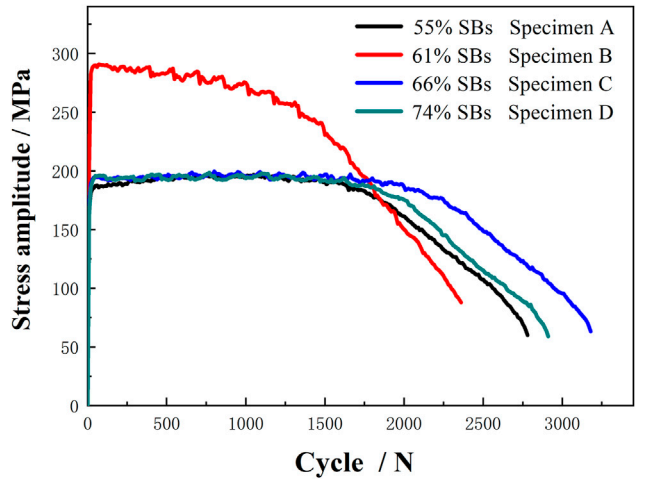

FIGURE 6 | The cyclic stress response curves of the initial specimen (specimen A) and the GBE-treated specimens (specimen B to specimen D).

can be seen from the comparison between **Figures 5C and D** that the Σ3, Σ9, and Σ27 boundaries were generated and the RHABs no longer existed due to the grain boundaries' reaction. It was conducive to increase the proportion of the SBs. From the position of the newly generated Σ9 boundary in **Figure 3**, it could be observed that the Σ9 boundary was generated by the reaction of the two Σ3 boundaries. Similarly, the Σ27 boundary was generated by the grain boundary reaction of Σ3 and Σ9. The formula of the grain boundary reactions is shown in **Eqs 1**, **2**.

$$\Sigma 3 + \Sigma 3 \rightarrow \Sigma 9 \quad (1)$$

$$\Sigma 3 + \Sigma 9 \rightarrow \Sigma 27 \quad (2)$$

This could explain that the growth trend of the (Σ9 + Σ27)/Σ3 value was similar to that of the SBs percentage. When the annealing time increased from 10 to 90 min, the Σ3 boundaries migrated frequently. It led to the generation of a large number of Σ9 and Σ27 boundaries. Meanwhile, the generated SBs became parts of the grain boundary network. As a result, the whole SB percentage increased rapidly and the significantly disrupted network of RHAGBs was obtained. Therefore, the larger value of (Σ9 + Σ27)/Σ3 resulted in more SB reactions and higher degree of multiple twinning.

Effect of GBE on the CF Properties in High-Temperature and High-Pressure Water

The cyclic stress response curves measured by the corrosion fatigue tests are shown in **Figure 6**. The four specimens signed from A to D were the initial specimen and the specimens annealing for 10, 45, and 90 min, respectively. The corresponding SBs of the four specimens were 55%, 61%, 66%, and 74%, respectively. It could be seen that specimen B had the highest fatigue stress (the range of 270–290 MPa)

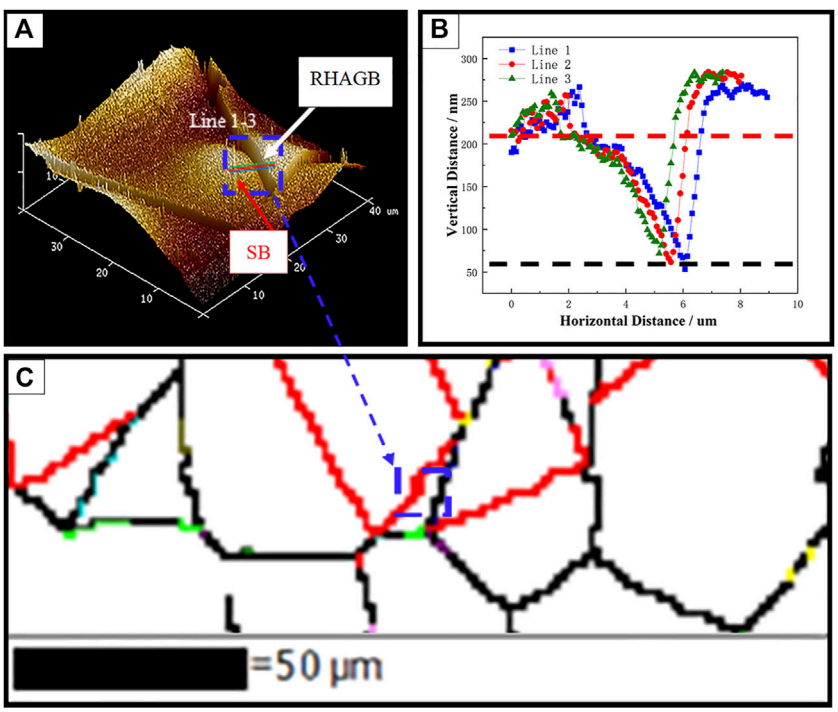

FIGURE 7 | Microstructure of the 316L ASS subjected to the intergranular corrosion: **(A)** AFM microstructure of the local area, **(B)** the corroded depth of the boundaries, and **(C)** the OIM map of GBCD.

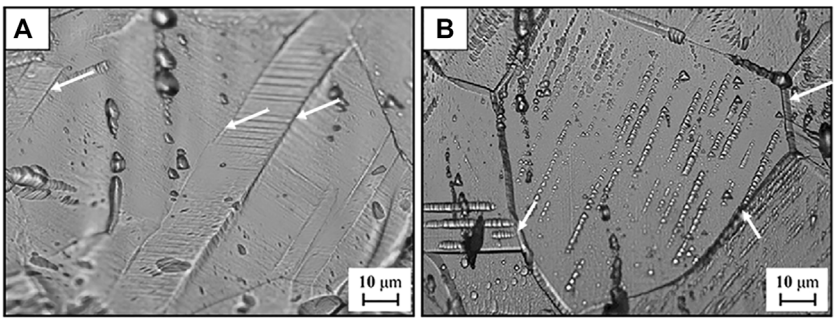

FIGURE 8 | The morphologies of the fatigue bands across the boundaries of **(A)** SBs and **(B)** RHAGBs.

and the shortest CF life (2,361 cycles). The fatigue stress of the other specimens was in the range of 190–195 MPa. The CF lives of specimen A and specimen D were 2,843 and 2,909 cycles, respectively. The longest CF life was 3,187 cycles in specimen C.

The driving force of the SB migration and SB reaction could be provided by the interfacial energy which was transformed from the deformation energy during the annealing. However, the annealing time (10 min) of specimen B was not enough to transform the storage energy into interfacial energy. The work hardening resulted in high hardness and low plasticity. In addition, the propagation of the corrosion path could not be prevented because the RHAGBs were still interconnected. Therefore, specimen B had the shortest life in the corrosion fatigue test.

To compare the corrosion resistance of the SB and the RHAGB, the depth of the corrosion ditches was measured by the atomic force microscope (AFM) morphology, as shown in **Figure 7**. As illustrated in **Figure 7B**, the vertical distances of the Σ3 boundary (red horizontal line) and the RHAGB (black horizontal line) were 210 and 60 nm, respectively. It meant that the corroded depth of the Σ3 boundary was much less than that of RHAGB. The relationship between the energy of a CSL boundary and that of a random boundary can be indicated by **Eq. 3**.

$$\gamma_{\Sigma} = \left(1 - \frac{1}{\sqrt{\Sigma}}\right)\gamma_{\mathrm{Random}} \tag{3}$$

where γ_{Σ} is the energy of a CSL boundary of notation Σ, and γ_{Random} is the energy of a random boundary.

The effective grain boundary energy (EGBE) was proposed as a guide to optimize the types of CSL boundaries and the grain size, as shown in **Eq. 4**.

$$\mathrm{EGBE} = \left[\left(\sum \mathrm{F_i}\gamma_{\mathrm{i}}\left(\frac{\Delta\theta_i}{\theta_{\mathrm{Max}}}\right)\right)\left(\frac{4}{\mathrm{d}}\right)\right] \tag{4}$$

where $\mathrm{F_i}$ and γ_{i} are the percentage and the energy of a CSL boundary of type i, respectively. d is the grain size. $\triangle\theta_{\mathrm{i}}$ is the average deviation from the perfect CSL, and θ_{Max} is the maximum deviation allowed by Brandon's criteria. It could be known that the larger grain size and the more SBs led to the lower EGBE. The initial specimen A had the smallest grain size and the lowest SB percentage among the four specimens which led to high EGBE and low corrosion resistance. The crack tips of specimen A were corroded easily. As a result, a short CF life was obtained.

The specimen annealed for 90 min had the highest SB percentage and the largest grain size. It could be observed that the EGBE of specimen D was the lowest among the four specimens. The fatigue bands could be easily propagated across the SBs, as shown in the arrows of **Figure 8A**. In comparison, the propagation of fatigue bands could be effectively blocked by the RHAGBs, as shown in the arrows of **Figure 8B**. Though the SBs had strong intergranular corrosion resistance, the strength of these boundaries was not enough to resist the propagation of transgranular fatigue cracks. Thus, the excessive percentage of SBs led to the decline of the CF life.

The SB percentage of specimen C annealed for 45 min was 66%. The appropriate percentage of SBs and the interrupted network of RHAGBs could ensure that the specimen had both a strong corrosion resistance and fatigue resistance. Consequently, specimen C had the highest life of CF test, that is, 3,187 cycles.

CONCLUSION

The method and mechanism of GBE on the GBCD and corrosion fatigue properties of 316L ASS were studied. It could be observed that the SBs' frequency of the 5% deformation specimen was increased from 55% to 74% when the annealing time increased from 0 to 90 min. The Σ9 boundary was generated by the reaction of the Σ3 boundary and the Σ3 boundary. Similarly, Σ27 boundary was generated by the reaction of the Σ3 boundary and the Σ9 boundary. The highest corrosion fatigue life for 3,187 cycles was obtained when the thermomechanical processing parameters of the 316L ASS were of 5% deformation, annealing temperature of 1373 K, and annealing time of 45 min. Though the low-energy special boundaries had strong intergranular corrosion resistance, the strength of these boundaries was not enough to resist the propagation of transgranular fatigue cracks.

DATA AVAILABILITY STATEMENT

The original contributions presented in the study are included in the article/Supplementary Material. Further inquiries can be directed to the corresponding author.

AUTHOR CONTRIBUTIONS

CZ, data curation and formal analysis. HW, microstructure analysis. BY, supervision. All authors contributed to manuscript revision and read and approved the submitted versions.

REFERENCES

Deepak, K., Mandal, S., Athreya, C. N., Kim, D.-I., de Boer, B., and Sarma, V. S. (2016). Implication of Grain Boundary Engineering on High Temperature Hot Corrosion of Alloy 617. *Corros. Sci.* 106, 293–297. doi:10.1016/j.corsci.2016.01.019

Engelberg, D. L., Newman, R. C., and Marrow, T. J. (2008). Effect of Thermomechanical Process History on Grain Boundary Control in an Austenitic Stainless Steel. *Scr. Mater.* 59 (5), 554–557. doi:10.1016/j.scriptamat.2008.05.012

Gao, Y., Ritchie, R. O., Kumar, M., and Nalla, R. K. (2005). High-Cycle Fatigue of Nickel-Based Superalloy ME3 at Ambient and Elevated Temperatures: Role of Grain-Boundary Engineering. *Metall. Mat. Trans. A* 36 (12), 3325–3333. doi:10.1007/s11661-005-0007-5

Gao, Y., Stölken, J. S., KumarRitchie, M. R. O., and Ritchie, R. O. (2007). High-Cycle Fatigue of Nickel-Base Superalloy René 104 (ME3): Interaction of Microstructurally Small Cracks with Grain Boundaries of Known Character. *Acta Mater.* 55 (9), 3155–3167. doi:10.1016/j.actamat.2007.01.033

Gao, J., Tan, J., Wu, X., and Xia, S. (2019). Effect of Grain Boundary Engineering on Corrosion Fatigue Behavior of 316LN Stainless Steel in Borated and Lithiated High-Temperature Water. *Corros. Sci.* 152, 190–201. doi:10.1016/j.corsci.2019.01.036

Gertsman, V. Y., and Bruemmer, S. M. (2001). Study of Grain Boundary Character Along Intergranular Stress Corrosion Crack Paths in Austenitic Alloys. *Acta Mater.* 49 (9), 1589–1598. doi:10.1016/S1359-6454(01)00064-7

Kang, S., Jeong, S., and Ahn, Y.-S. (2021). Effect of Discontinuous Yielding on the Strain Hardening Behavior of Fine-Grained Twinning-Induced Plasticity Steel. *Front. Mat.* 8, 28. doi:10.3389/fmats.2021.599534

Kobayashi, S., Hirata, M., Tsurekawa, S., and Watanabe, T. (2011). Grain Boundary Engineering for Control of Fatigue Crack Propagation in Austenitic Stainless Steel. *Procedia Eng.* 10, 112–117. doi:10.1016/j.proeng.2011.04.021

Kobayashi, S., Yang, W., Tomobe, Y., Okada, R., and Tsurekawa, S. (2020). Low-Angle Boundary Engineering for Improving High-Cycle Fatigue Property of 430 Ferritic Stainless Steel. *J. Mater. Sci.* 55 (22), 9273–9285. doi:10.1007/s10853-020-04555-0

Lehockey, E. M., Palumbo, G., Lin, P., and Brennenstuhl, A. M. (1997). On the Relationship between Grain Boundary Character Distribution and Intergranular Corrosion. *Scr. Mater.* 36 (10), 1211–1218. doi:10.1016/S1359-6462(97)00018-3

Lehockey, E. M., Palumbo, G., and Lin, P. (1998). Improving the Weldability and Service Performance of Nickel-And Iron-Based Superalloys by Grain Boundary Engineering. *Metall. Mat. Trans. A* 29 (12), 3069–3079. doi:10.1007/s11661-998-0214-y

Li, Q., Cahoon, J. R., and Richards, N. L. (2009). Effects of Thermo-Mechanical Processing Parameters on the Special Boundary Configurations of Commercially Pure Nickel. *Mater. Sci. Eng. A* 527 (1-2), 263–271. doi:10.1016/j.msea.2009.07.064

Mohtadi-Bonab, M. A., Eskandari, M., Sanayei, M., and Das, S. (2018). Microstructural Aspects of Intergranular and Transgranular Crack Propagation in an API X65 Steel Pipeline Related to Fatigue Failure. *Eng. Fail. Anal.* 94, 214–225. doi:10.1016/j.engfailanal.2018.08.014

Shimada, M., Kokawa, H., Wang, Z. J., Sato, Y. S., and Karibe, I. (2002). Optimization of Grain Boundary Character Distribution for Intergranular Corrosion Resistant 304 Stainless Steel by Twin-Induced Grain Boundary Engineering. *Acta Mater.* 50 (9), 2331–2341. doi:10.1016/S1359-6454(02)00064-2

Sinha, S., Kim, D.-I., Fleury, E., and Suwas, S. (2015). Effect of Grain Boundary Engineering on the Microstructure and Mechanical Properties of Copper Containing Austenitic Stainless Steel. *Mater. Sci. Eng. A* 626, 175–185. doi:10.1016/j.msea.2014.11.053

Spigarelli, S., Cabibbo, M., Evangelista, E., and Palumbo, G. (2003). Analysis of the Creep Strength of a Low-Carbon AISI 304 Steel with Low-Σ Grain Boundaries. *Mat. Sci. Eng. A-Struct.* 352 (1-2), 93–99. doi:10.1016/S0921-5093(02)00903-6

Thaveeprungsriporn, V., and Was, G. S. (1997). The Role of Coincidence-Site-Lattice Boundaries in Creep of Ni-16Cr-9Fe at 360 °C. *Metall. Mat. Trans. A* 28 (10), 2101–2112. doi:10.1007/s11661-997-0167-6

Wang, Z. C., Paschalidou, E. M., Seyeux, A., Zanna, S., Maurice, V., and Marcus, P. (2019). Mechanisms of Cr and Mo Enrichments in the Passive Oxide Film on 316L Austenitic Stainless Steel. *Front. Mater.* 6, 1–12. doi:10.3389/fmats.2019.00232

Watanabe, T. (1984). An Approach to Grain Boundary Design for Strong and Ductile Polycrystals. *Res. Mech.* 11 (1), 47–84.

Watanabe, T., and Tsurekawa, S. (1999). The Control of Brittleness and Development of Desirable Mechanical Properties in Polycrystalline Systems by Grain Boundary Engineering. *Acta Mater.* 47 (15-16), 4171–4185. doi:10.1016/S1359-6454(99)00275-X

West, E. A., and Was, G. S. (2009). IGSCC of Grain Boundary Engineered 316L and 690 in Supercritical Water. *J. Nucl. Mater.* 392 (2), 264–271. doi:10.1016/j.jnucmat.2009.03.008

Conflict of Interest: CZ is employed by China Nerin Engineering Company Limited, HW is employed by Suzhou Nuclear Power Research Institute Company Limited.

The remaining authors declare that the research was conducted in the absence of any commercial or financial relationships that could be construed as a potential conflict of interest.

Publisher's Note: All claims expressed in this article are solely those of the authors and do not necessarily represent those of their affiliated organizations, or those of the publisher, the editors, and the reviewers. Any product that may be evaluated in this article, or claim that may be made by its manufacturer, is not guaranteed or endorsed by the publisher.